

THE FORMATION OF SPHEROIDS IN EARLY-TYPE SPIRALS: CLUES FROM THEIR GLOBULAR CLUSTERS*

APARNA MAYBHATE¹, PAUL GOUDFROOIJ¹, RUPALI CHANDAR², AND THOMAS H. PUZIA³

¹ Space Telescope Science Institute, 3700 San Martin Drive, Baltimore, MD 21218, USA

² Department of Physics and Astronomy, The University of Toledo, Toledo, OH 43606, USA

³ Herzberg Institute of Astrophysics, 5071 West Saanich Road, Victoria, BC V9E 2E7, Canada

Received 2010 May 11; accepted 2010 August 3; published 2010 September 1

ABSTRACT

We use deep *Hubble Space Telescope* images taken with the Advanced Camera for Surveys (ACS) in the F475W and F814W filters to investigate the globular cluster (GC) systems in four edge-on Sa spiral galaxies covering a factor of four in luminosity. The specific frequencies of the blue GCs in the galaxies in our sample fall in the range 0.34–0.84, similar to typical values found for later-type spirals. The number of red GCs associated with the bulges generally increases with the bulge luminosity, similar to what is observed for elliptical galaxies, although the specific frequency of bulge clusters is a factor of 2–3 lower for the lowest luminosity bulges than for the higher-luminosity bulges. We present a new empirical relation between the fraction of red GCs and total bulge luminosity based on the elliptical galaxies studied by ACSVCS (ACS Virgo Cluster Survey) and discuss how this diagram can be used to assess the importance of dissipative processes in building spiral bulges. Our results suggest a picture where dissipative processes, which are expected during gas-rich major mergers, were more important for building luminous bulges of Sa galaxies, whereas secular evolution may have played a larger role in building lower-luminosity bulges in spirals.

Key words: galaxies: bulges – galaxies: spiral – galaxies: star clusters: general

Online-only material: color figure

1. INTRODUCTION

The assembly history of spiral galaxies remains one of the most pressing questions in astrophysics today (e.g., Kormendy & Kennicutt 2004). In particular, we do not have a clear picture of the formation mechanism for the central bulges of spiral galaxies. In the early universe, galactic evolution was primarily driven by violent merging and dissipative collapse. Mergers are accompanied by dissipation and star formation and are believed to make classical bulges and elliptical galaxies. Are bulges of spirals simply “small ellipticals,” having formed through vigorous star formation through short timescale dissipative processes or merging during the early universe, with disks assembled later on? Or is bulge formation through secular evolution of inner disk stars a more common mechanism? Secular evolution is a slow process and involves the redistribution of disk material. In this scenario, material is driven into the galaxy center by means of a bar instability (e.g., Pfenniger & Norman 1990; Sheth et al. 2005) or a minor interaction with a small satellite galaxy (up to 10% of the main galaxy mass; see Pfenniger 1999), triggering low-level star formation. As a result, galaxies would evolve from late types to early types with the growth of their bulges. A relatively new and powerful way to probe these fundamental questions is the study of the spheroids and their associated globular cluster (GC) systems in early-type spiral galaxies.

In “normal” elliptical galaxies, previous *Hubble Space Telescope* (HST) studies have shown that the broadband color distributions of the GC systems are more consistent with two subpopulations of star clusters. Under the assumption that the GCs in these systems have ages greater than a few gigayears, this color difference indicates the presence of two GC populations

of different metallicities: blue (metal-poor) and red (metal-rich) clusters (e.g., Gebhardt & Kissler-Patig 1999; Kundu & Whitmore 2001; Larsen et al. 2001; Peng et al. 2006). The specific frequency of GCs (S_N , the total number of GCs per unit galaxy luminosity) in “normal” ellipticals is high, typically in the range 1.5–4 (e.g., Peng et al. 2008). The spatial distribution and colors of massive metal-rich (red) GCs closely follow that of the spheroidal light (i.e., the “bulge”), whereas the metal-poor (blue) GC system is usually more extended (“halo-like;” Kundu & Whitmore 1998; Dirsch et al. 2003; Puzia et al. 2004; Rhode & Zepf 2004; Goudfrooij et al. 2007). This is generally interpreted as strong evidence that the formation of elliptical galaxies involved the formation of large numbers of such massive metal-rich GCs and hence that star formation occurred in a vigorous and rapid manner (“dissipative collapse”).

If the bulges of spirals formed in a manner similar to that in ellipticals, we expect galaxies with larger bulge-to-total luminosity ratios to be associated with a larger number of clusters. At face value, these results seem consistent with a relatively simple picture in which GC systems of spirals are made up of a “universal” halo population of metal-poor GCs that is present in each galaxy, plus a metal-rich bulge population which grows with the bulge mass or luminosity. On the other hand, in the “secular evolution” scenario, galaxies would evolve from late types to early types with the growth of their bulges, but the properties of their GC systems would remain largely unchanged because low star formation rates do not allow for the formation of star clusters that are massive enough to survive a Hubble time (e.g., Bastian 2008).

Studies of GC systems in spirals with Hubble types of Sb and later (Goudfrooij et al. 2003) and nearby face-on spirals (Chandar et al. 2004) showed that they have S_N values of 0.55 ± 0.25 , i.e., much lower than in ellipticals, whereas earlier-type spirals typically have higher S_N values (see also Georgiev et al. 2010). This scenario would indicate that spiral bulges

* Based on observations with the NASA/ESA *Hubble Space Telescope*, obtained at the Space Telescope Science Institute, which is operated by the Association of Universities for Research in Astronomy, Inc., under NASA contract NAS5-26555.

Table 1
Basic Properties of the Galaxy Sample

| Properties | NGC 5475 | NGC 4710 | NGC 5308 | NGC 4866 |
|------------------------|------------------|------------------|------------------|------------------|
| m-M | 32.3 | 31.0 | 32.4 | 32.3 |
| M_{B_0} | -19.05 | -19.20 | -20.17 | -20.57 |
| M_K | -22.89 | -23.43 | -24.04 | -24.38 |
| $(g - I)_{\text{KMM}}$ | 1.21, 1.53 | 1.37, 1.64 | 1.36, 1.79 | 1.43, 1.80 |
| $m_{I_{\text{TO}}}$ | 23.99 ± 0.09 | 22.65 ± 0.17 | 23.41 ± 0.06 | 24.13 ± 0.14 |
| $M_{I_{\text{TO}}}$ | -8.30 | -8.35 | -8.99 | -8.17 |
| n_{bulge} | 2.9 | 1.2 | 3.5 | 3.0 |
| S_N | 0.44 ± 0.12 | 0.78 ± 0.20 | 1.17 ± 0.31 | 1.07 ± 0.28 |
| $S_N(\text{blue})$ | 0.34 ± 0.09 | 0.61 ± 0.16 | 0.84 ± 0.22 | 0.63 ± 0.16 |
| Red fraction | 0.23 ± 0.06 | 0.21 ± 0.06 | 0.28 ± 0.05 | 0.38 ± 0.05 |
| B/T | 0.60 | 0.48 | 0.53 | 0.47 |
| $(g - I)_{\text{div}}$ | 1.50 | 1.50 | 1.55 | 1.60 |
| $r_{\text{s,e}}$ | 3.95 | 2.96 | 2.96 | 12.30 |

Notes. Row (1): object ID. Row (2): distance moduli calculated using velocity from <http://nedwww.ipac.caltech.edu> (NED) and assuming $H_0 = 70 \text{ km s}^{-1} \text{ Mpc}^{-1}$. Row (3): absolute B magnitude from NED. Row (4): absolute K magnitude from NED. Row (5): $g - I$ values of the peaks detected by KMM within 14 kpc. Row (6): the magnitude at the turnover of the LF in the I band. Row (7): the absolute magnitude of the turnover in the I band. Row (8): Sérsic index of the bulge. Row (9): the total specific frequency for the GCs. Row (10): the specific frequency of the blue clusters alone. Row (11): the fraction of the red clusters obtained by dividing the number of red clusters by the total number of clusters. Row (12): bulge to total luminosity ratio of the galaxy in the I band. Row (13): $g - I$ color to divide “blue” from “red” clusters. Row (14): effective radius of the bulge in arcsecs.

are like small ellipticals having formed early on through rapid dissipative collapse and now residing at the center of a large disk which was mostly assembled later. Based on properties of GC systems in the Milky Way, M31, and M104, Forbes et al. (2001) suggested that red, metal-rich GCs in spirals are associated with bulges and are the direct analogs of the red GCs seen in ellipticals. If this association can be verified and established, this would provide an important causal link between the formation of metal-rich GCs and that of spheroidal systems (i.e., bulges and ellipticals). Thus, a thorough study of GC systems in spirals can provide important new clues regarding the formation of bulges/spheroids in spiral galaxies.

In the simple picture described above, the unambiguous detection of a relationship between bulge luminosity/mass and the specific frequency of GCs is highly dependent on the results for bulge-dominated spirals (i.e., Sa galaxies) but studies of GC systems of Sa galaxies are still rather sparse. In this paper, we test the two basic scenarios for the formation of bulges in Sa galaxies: (1) vigorous star (and cluster) formation through rapid dissipative processes which could be triggered by merging and (2) the slow secular evolution accompanied by low levels of star formation. We present the results of a new study of the GC systems of four edge-on, bulge-dominated (early-type) spiral galaxies. We focus on the GC color distributions and the relations between the GC specific frequency S_N and host galaxy luminosity as well as the bulge-to-total luminosity ratio.

2. OBSERVATIONS AND ANALYSIS OF *HST*/ACS DATA

As part of *HST* program GO-10594 (PI: Goudfrooij), we selected four nearby, edge-on, bulge-dominated spiral galaxies to study their GC systems. All these galaxies have the same morphological type (Sa), and they span a factor of ~ 4 in luminosity. The basic properties of our target galaxies, including

their distance and absolute magnitude in the B and K bands, are given in Table 1.

Observations were made using the Wide Field Channel (WFC) of the Advanced Camera for Surveys (ACS) aboard the *HST* in the F475W and F814W filters. The WFC has a $202'' \times 202''$ field of view with a plate scale of $0''.05 \text{ pixel}^{-1}$. We chose these filters as the best compromise between high sensitivity and long color baseline. Total exposure times ranged from 1164 s to 3820 s in F475W and from 1000 s to 2320 s in F814W. The flat-fielded images produced by the *HST* pipeline were run through the task MULTIDRIZZLE, with the background subtraction turned off, resulting in geometrically corrected images with most cosmic rays removed. These images are shown in Figure 1.

Object detection was done following the general procedure described in Maybhate et al. (2007). First, we removed the strong and varying galaxy light by applying a circular median filter of radius 15 pixels and dividing the image in each filter by the square root of this median image thus providing uniform shot-noise characteristics over the whole frame. Object finding was done on the square-root-divided images in each filter. We detected sources in our images using the DAOFIND task in IRAF using a detection threshold of 4σ above the background.

Next, we selected candidate GCs from the source lists by separating them from foreground stars and background galaxies based on their colors and morphology. Total magnitudes of these sources were measured and transformed from the STAG to the Sloan Digital Sky Survey (SDSS) g and Cousins I band using the SYNPHOT package within STSDAS (see Maybhate et al. 2007). Our final selection of cluster candidates was done based on the following criteria.

1. $1.1 \leq g - I \leq 2.2$.
2. M_I brighter than 1.0 mag beyond the expected turnover of the luminosity function (LF; $M_{I_{\text{TO}}} = -8.46$; Kundu & Whitmore 2001).
3. $1.5 \text{ pixels} \leq \text{FWHM} \leq 5.0 \text{ pixels}$.
4. $0.9 \leq \text{magnitudes between aperture radii of } 1 \text{ pixel and } 3 \text{ pixels} \leq 1.6$.

We apply the criteria for both the FWHM and the concentration index since we previously found that using only one of these does not fully reject extended sources (see Figure 1 in Goudfrooij et al. 2007). We perform artificial cluster experiments to determine the completeness of our samples by randomly distributing synthetic point sources with magnitudes between 22.0 and 28.0 over five distinct background levels in the I -band image for each galaxy. Batches of 100 sources each were added and recovered from each image in brightness intervals of 0.25 mag. See Maybhate et al. (2007) for details of this procedure.

Sources with completeness fractions $\geq 50\%$ were selected to make the final list of GCs. The final lists contain 44, 63, 191, and 273 clusters for NGC 5475, NGC 4710, NGC 5308, and NGC 4866, respectively.

3. STRUCTURAL PARAMETERS FOR TARGET GALAXIES

We use the *HST* images to determine the ratio of bulge to total luminosity (B/T) for each galaxy. Bulge parameters were derived for each galaxy using the I -band image, and the bulge/disk decomposition method described in Goudfrooij et al. (2003) with one exception. Rather than fitting an exponential profile (representing a disk) plus a de Vaucouleurs (1953) $r^{1/4}$ profile (representing a bulge) to the observed minor-axis profile of

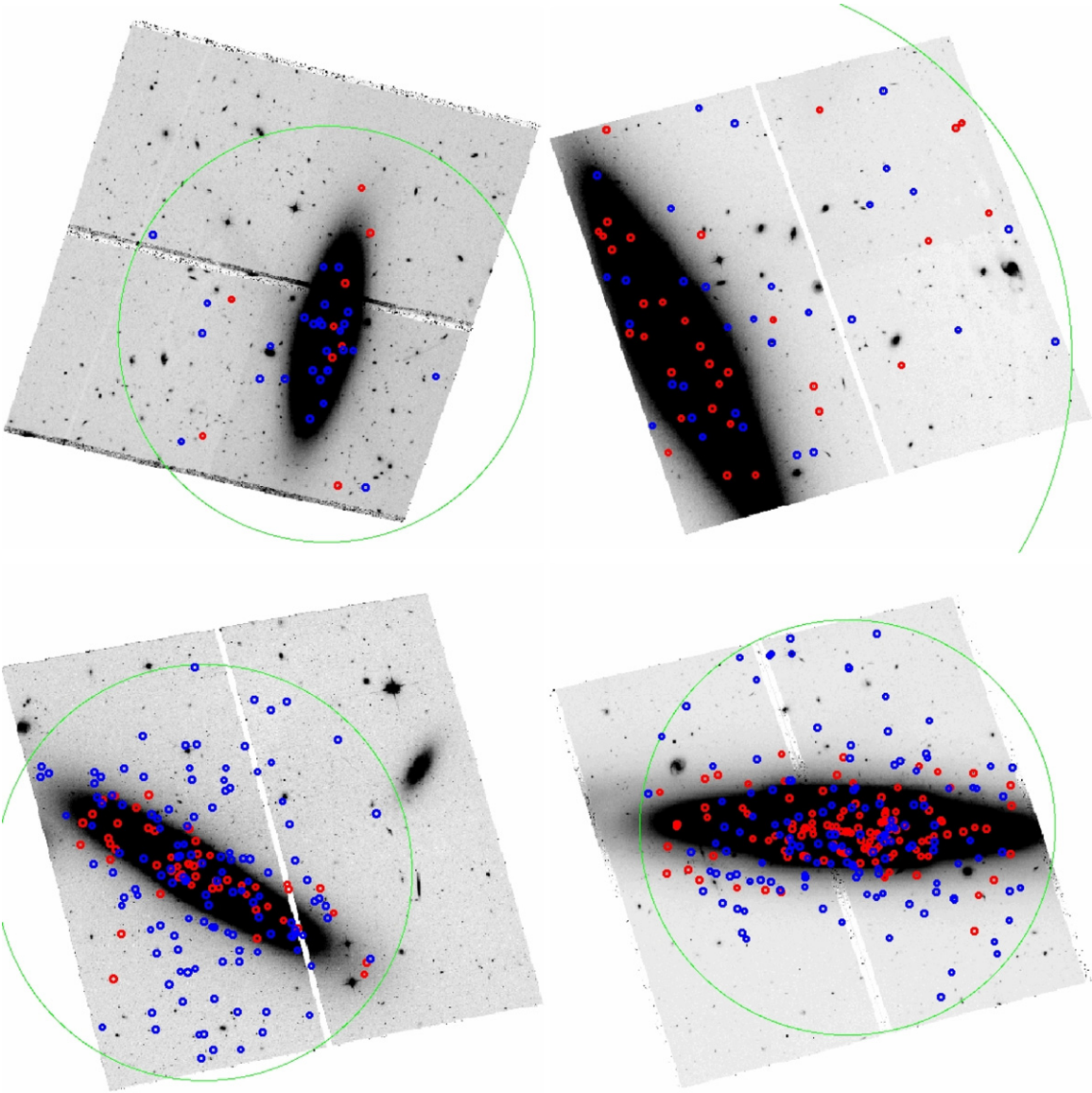


Figure 1. Positions of clusters superposed on the *I*-band ACS/WFC images of (clockwise from top left) NGC 5475, NGC 4710, NGC 4866, and NGC 5308. See the text for definitions of red and blue clusters. The green curve is a circle of radius 14 kpc drawn around the galaxy center. North is to the top and east is to the left.

the galaxies, we fit an exponential profile plus a Sérsic (1963) profile

$$\Sigma_S(z) = \Sigma_{s,e} \exp\{-a [(z/z_{s,e})^{1/n} - 1]\}, \quad (1)$$

where $z_{s,e}$ is the Sérsic effective radius along the minor axis, a is a scale factor, $\Sigma_{s,e}$ is the intensity at $z = z_{s,e}$, and n is the Sérsic parameter indicating the slope of the bulge profile. The fit was done by means of an iterative nonlinear minimization routine after making initial estimates of the fit parameters using bootstrap tests. Areas where dust extinction is apparent in the image were flagged and ignored during the fitting process. Minor-axis $z_{s,e}$ values were converted to bulge effective radii $r_{s,e} = z_{s,e}/\sqrt{1-\epsilon}$, where ϵ is the ellipticity of the bulge as derived from ellipse fits to the *I*-band image (using the STSDAS task ELLIPSE). Total bulge luminosities B were then derived using

$$B = 22.7 \exp(2n - 0.324 - a) \Sigma_{s,e} r_{s,e}^2$$

(cf. Ciotti 1991).

Since these galaxies do not entirely fit on the ACS/WFC images, it is not possible to estimate the total *I*-band luminosity using our images alone. Assuming that the photometric growth curves of the target galaxies are the same for *I* as for *J*, since these two bands are reasonably close in wavelength, we apply the aperture correction from 14'' to infinity that is available from the Two Micron All Sky Survey catalog to derive the total *I*-band magnitude for each galaxy. B/T values were determined for each galaxy from these values for the total luminosity and the bulge luminosity computed above. Resulting values for $r_{s,e}$, n , and B/T are listed in Table 1.

4. COLOR DISTRIBUTIONS OF THE GLOBULAR CLUSTERS

Many GC systems have bimodal color distributions, which provide important clues to the formation of the host galaxies. Since most previous studies of GC systems used $V-I$ colors, we transformed $V-I$ to $g-I$ using the GALEV simple stellar population models (Anders & Fritze-v. Alvensleben 2003) for

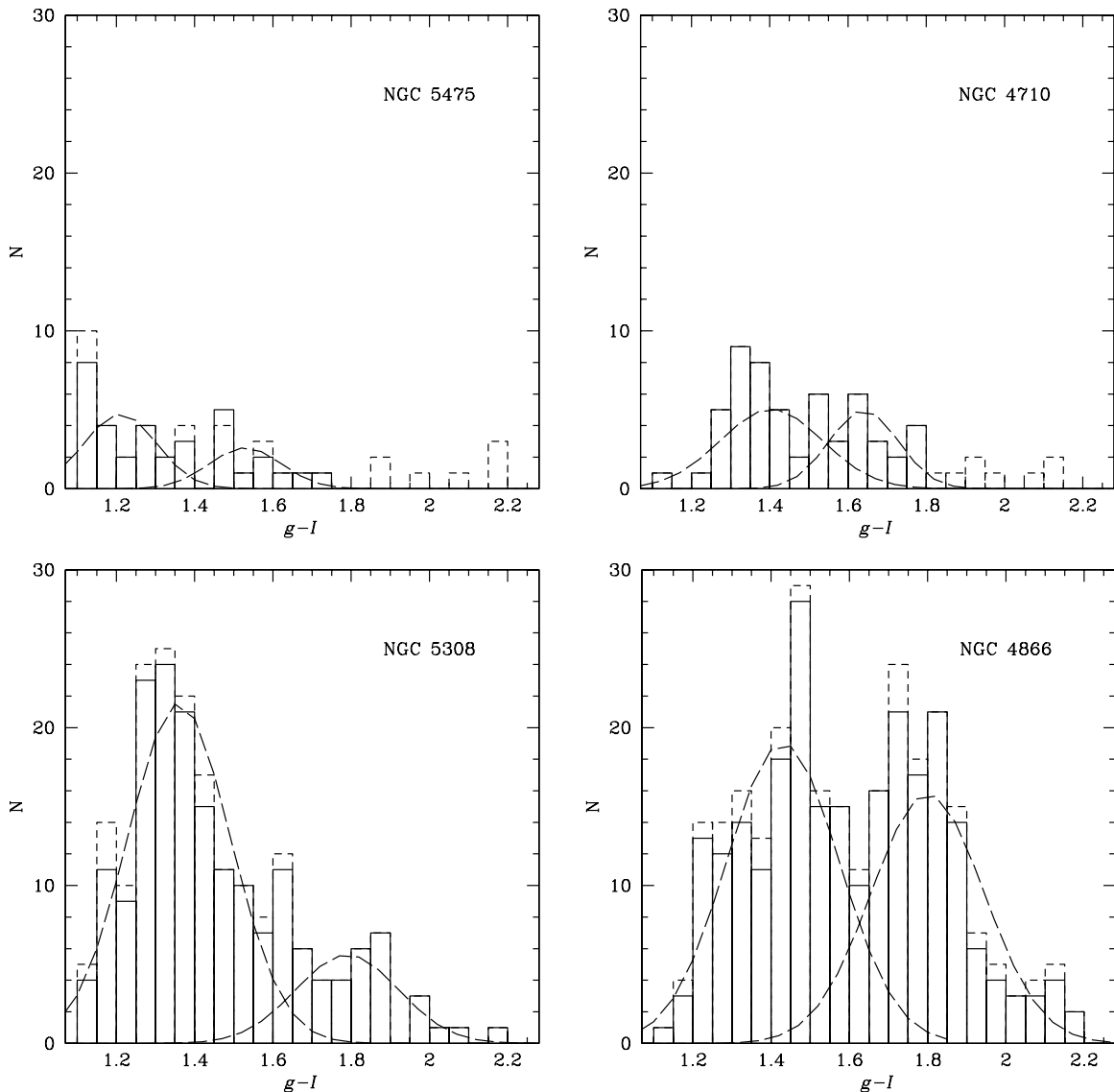


Figure 2. GC color distributions for our target galaxy sample. The histograms with solid lines represent the color distribution within the inner 14 kpc in each galaxy. The dashed curves are the estimates from KMM while the dotted histograms represent the total number of clusters detected in the entire image.

an assumed age of 13 Gyr. The GALEV models are calibrated to the ACS filters and treat the chemical evolution of the gas and the spectral evolution of the stellar content simultaneously. They also include absorption as well as emission, both line and continuum. Using the results of Larsen et al. (2001), we find that typical peaks for GC systems in E/S0 galaxies are expected to occur at $g - I$ values of 1.35–1.40 for the blue (metal-poor) clusters (see also Maybhate et al. 2007, 2009) and 1.72–1.85 for the red (metal-rich) clusters. Using the bulge luminosities of our sample galaxies, the linear relations between peak $V - I$ color (for both blue GCs and red GCs) and elliptical galaxy luminosity of Larsen et al. (2001) are used to predict $g - I$ colors to divide “blue” and “red” clusters. These colors are listed in Table 1. Figure 1 shows the positions of the red and blue cluster candidates on the I -band ACS image.

NGC 4710 is the nearest galaxy ($m - M = 31.0$) while the other three are more distant by a factor of 3–4. As a result, the ACS image of NGC 4710 covers the smallest radial extent (~ 14 kpc). Therefore, we only consider GCs that lie within 14 kpc in all galaxies and investigate whether or not their color distributions are bimodal using the KMM algorithm (McLachlan

& Basford 1988; Ashman et al. 1994). We kept the dispersions the same for the two Gaussians and found that the p -value ranged from 0.00 to 0.018. Low p -values reject the hypothesis that the examined distribution resulted from a single Gaussian distribution. Histograms of the $g - I$ color distributions within 14 kpc and the KMM fits are shown in Figure 2. In all four target galaxies, we detect a dominating blue GC population at $g - I \approx 1.4$. This is consistent with the old, metal-poor cluster population seen in normal elliptical galaxies. We also clearly detect a redder population at $g - I \approx 1.8$ in the more luminous galaxies, NGC 5308 and NGC 4866, and at $g - I \approx 1.6$ in the less luminous galaxy, NGC 4710. NGC 5475 does not show a significant red GC population. The peaks detected by the KMM algorithm are given in Table 1. The red peak colors at $g - I \approx 1.8$ and 1.6 are consistent with the colors of old, metal-rich clusters seen in elliptical galaxies with similar (bulge) luminosities (Larsen et al. 2001; Peng et al. 2006). Reddening does not seem to be significant in the galaxies and we do not expect that any reddened “blue” clusters were classified as “red” since the KMM shows a clear bimodality. Had the blue clusters been reddened considerably, we would have expected to see more

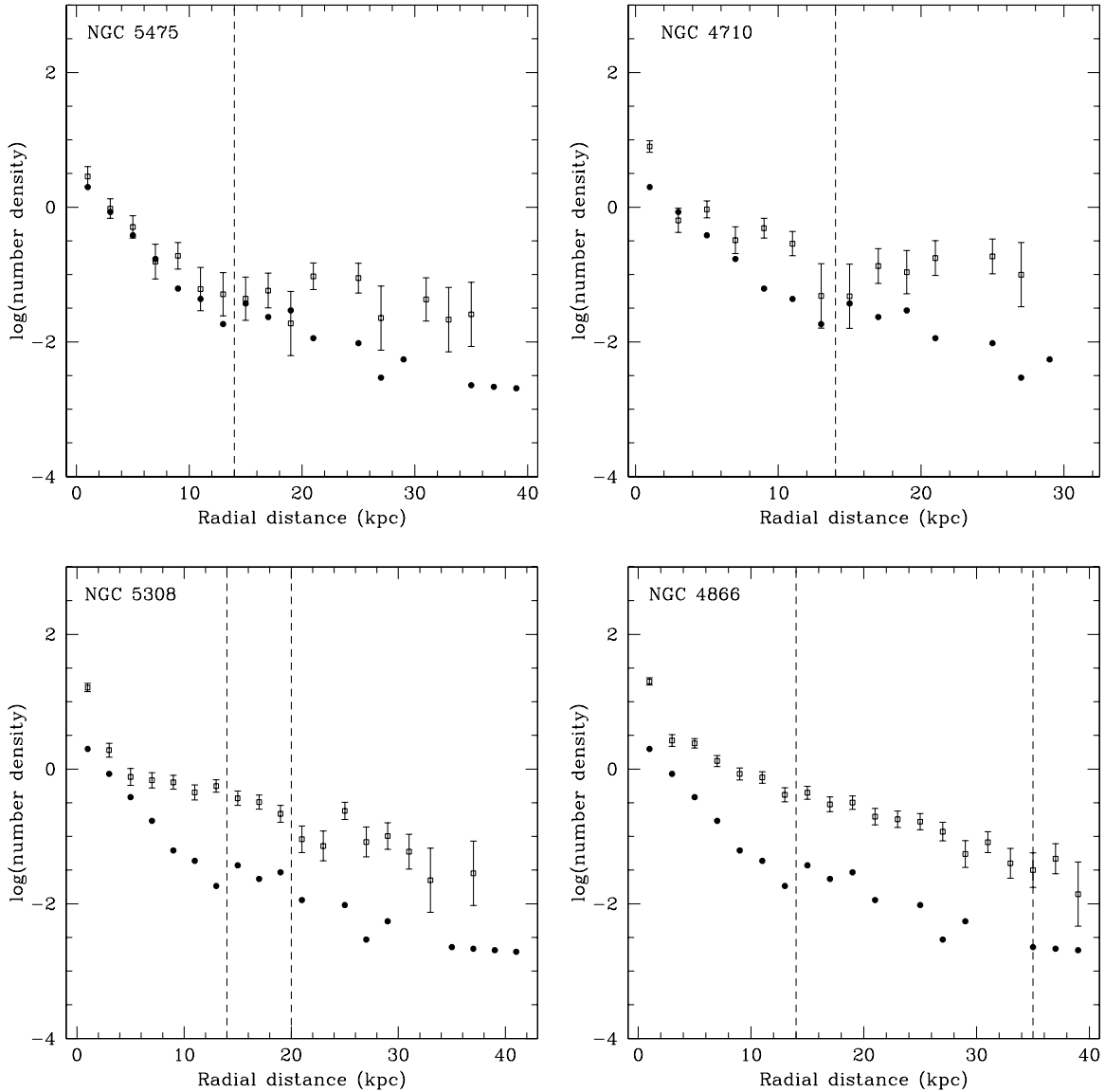


Figure 3. Log of the surface number density per square kiloparsec of the GCs as a function of radial distance from the center of the galaxy. Open squares and filled circles denote the values for the target galaxy and the Milky Way, respectively. Vertical dashed lines are drawn at 14 kpc and at the extent of the GC system of each target galaxy.

clusters in the valley between the two Gaussians and not a clear bimodality. A measurement of potential reddening in ellipticals by Goudfrooij & de Jong (1995), using IRAS (infrared) data and optical colors, showed that any color gradient is small, with $B - I$ below 0.03 per dex. These results for ellipticals suggest that reddening should not significantly affect the colors of clusters in early-type galaxies, such as the ones studied here.

5. SPECIFIC FREQUENCY OF GLOBULAR CLUSTERS

We constructed the GC LFs for the galaxies within the inner 14 kpc in the I band after completeness corrections and determined turnover magnitudes ($M_{I_{TO}}$) by means of a Gaussian fit.

The total number of clusters within 14 kpc was computed by doubling the number of observed clusters brighter than $M_{I_{TO}}$ (cf. Harris & van den Bergh 1981) for all galaxies except NGC 5308 for which we used $M_{I_{TO}} = -8.46$ since it showed a much brighter $M_{I_{TO}}$ (see Table 1). Correction for incomplete spatial coverage within 14 kpc was done by assuming a symmetric cluster distribution. Using M/L ratios and the relation between

the spatial extent of GCs and the mass of the galaxy from Rhode et al. (2007), we estimate the extent of their GC systems to be ~ 14 kpc (NGC 5475 and NGC 4710), 20 kpc (NGC 5308), and 35 kpc (NGC 4866). It is clear from Figure 1 that we do not sample the full azimuthal extent of the GC system beyond a radius of 14 kpc in NGC 5308 and NGC 4866. In Figure 3, we show the number density (number of clusters per square kiloparsec) versus the radial distance from the center of the galaxy for each target galaxy for the entire radial coverage in the ACS image. We have also added the number density profile for the Milky Way for comparison. The bottom panels of Figure 3 show that the radial density profiles of GCs from 14 to 20 kpc in NGC 5308 and from 14 to 35 kpc in NGC 4866 are similar to that in the Milky Way. Hence, we used a (scaled) extrapolation of the GC system beyond 14 kpc from the Milky Way profile.

Using the radial distribution of the metal-poor and metal-rich Galactic GCs as determined from the current version of the Harris (1996) catalog, we then estimate the total number of GCs in each of our sample galaxies and calculate the total specific frequency (S_N) of the GC systems. S_N is defined as the number

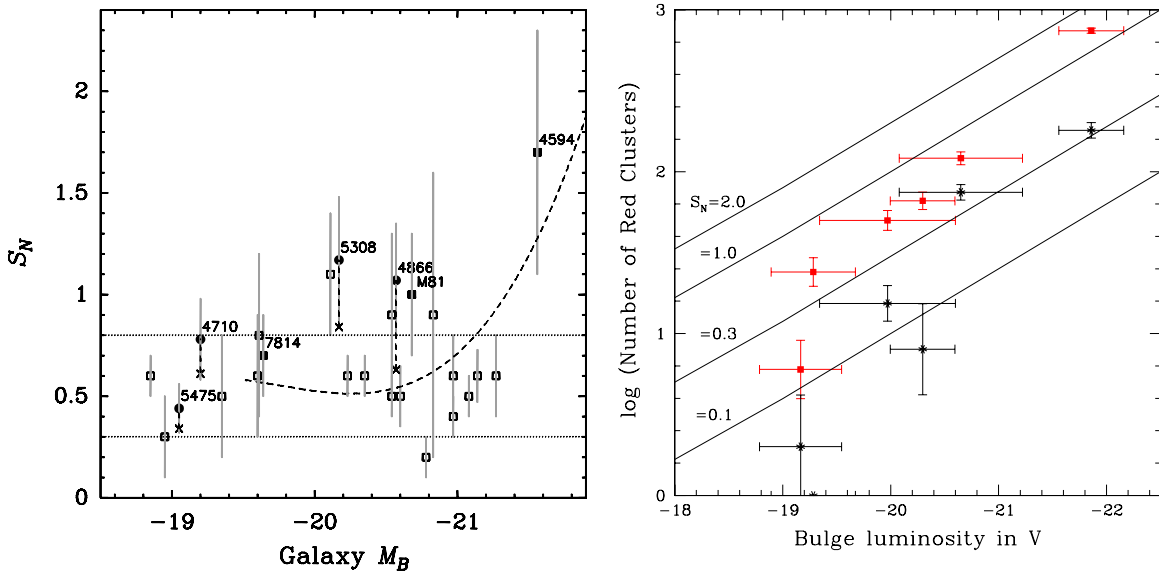


Figure 4. Left: relation between the galaxy B luminosity and specific frequency. The filled circles denote the total S_N for the sample galaxies while the crosses are the S_N values for the blue clusters alone. The filled squares and the open squares show the total S_N values for early-type and late-type spirals, respectively, taken from Goudfrooij et al. (2003), Rhode et al. (2007), and Chandar et al. (2004). The dotted lines show the range of values seen for the total S_N in late-type spirals (Goudfrooij et al. 2003) while the dashed line depicts a least-squares fit to the S_N of blue clusters (Rhode et al. 2007). Right: the number of red clusters as a function of the bulge V luminosity. The filled squares represent all the red clusters while the black asterisks represent the number of clusters within $2 R_{\text{eff}}$. The solid lines show relations for $S_N = 0.1, 0.3, 1.0,$ and 2.0 .

(A color version of this figure is available in the online journal.)

of star clusters per galaxy luminosity normalized to an absolute V magnitude of -15 (Harris & van den Bergh 1981). We also compute S_N for blue clusters alone. See Table 1 for results.

We could not find a V magnitude for NGC 5475 in the literature so we interpolated the SDSS $ugriz$ magnitudes and then converted the interpolated ABMAG to a Vega-based V magnitude. The left panel of Figure 4 shows the relation between the total B luminosity of each galaxy and S_N . For our sample galaxies, values for both the total S_N and the blue S_N are shown. Total S_N values for early-type and late-type spirals from Goudfrooij et al. (2003), Rhode et al. (2007), and Chandar et al. (2004) are also shown. We see that our blue S_N values (0.34–0.84) mostly lie within the typical S_N values for late-type spirals (0.55 ± 0.25) found by these authors. This strengthens the argument that GC systems of spirals are made of a universal halo population of metal-poor GCs that are present in all galaxies.

6. DISCUSSION

Here, we focus on using the properties of the red GCs to better understand bulge assembly. The right panel of Figure 4 shows the relation between bulge luminosity and the total number of red GCs (red symbols), as well as the number of red GCs located within $2 R_{\text{eff}}$ of the bulge (“bulge” GCs; asterisks), for our sample plus the Sa galaxies NGC 4594 (Spitler et al. 2006) and NGC 7814 (Goudfrooij et al. 2003). The total number of red GCs and bulge GCs clearly increases with bulge luminosity. The superimposed lines of constant specific frequency (S_N) show that the specific frequency does not remain constant but changes with bulge luminosity. Low-luminosity bulges (with $M_V \geq -20$) have lower values of S_N than higher-luminosity bulges. Secular evolution leads to an increase in bulge luminosity without a corresponding increase in the number of bulge clusters, since the low star formation rates associated with the secular building

of bulges (e.g., Sheth et al. 2005) do not lead to the formation of clusters massive enough to survive a Hubble time (Bastian 2008). Secular evolution therefore predicts no trend in the number of bulge clusters with bulge luminosity. On the other hand, bulge assembly through vigorous star formation events such as those occurring during mergers or interactions of gas-rich galaxies is known to be associated with the formation of massive star clusters (e.g., Whitmore & Schweizer 1995; Schweizer et al. 1996; Miller et al. 1997; Goudfrooij et al. 2001, 2004, 2007). Since the right panel of Figure 4 indicates that the number of bulge clusters increases with bulge luminosity (especially among the more luminous bulges), it seems fair to conclude that vigorous star formation events dominated secular evolution during the assembly history of those bulges.

Disruption of GCs, on both long and short timescales, can potentially affect S_N . We first consider the two disruption processes that have the most significant impact on the long-term survival of bulge GCs: two-body relaxation (sometimes called “evaporation”) and dynamical friction (e.g., Gnedin & Ostriker 1997; Fall & Zhang 2001; Vesperini 2001; Prieto & Gnedin 2008). We only consider GCs brighter than or equal to the turnover luminosity, corresponding to a mass of $\approx 2 \times 10^5 M_\odot$ for an age of 12 Gyr (e.g., McLaughlin & Fall 2008), since these are the only clusters used in the S_N calculation. For evaporation, we use the simple parameterization of McLaughlin & Fall (2008), which evolves an initial Schechter function over time, at rates that depend on the internal density of the clusters. Differences in age have a small effect on S_N , at the $\approx 10\%$ level, since for a typical density, the number of clusters more massive than the turnoff decreases by only 12% between 1.5 and 12 Gyr and by 9.8% between 3 and 12 Gyr. Based on the data presented in Jordán et al. (2005), the sizes of red GCs are similar in the low- and high-luminosity bulges of elliptical and S0 galaxies, over a similar range of cluster luminosities. This suggests that the internal densities, and hence the evaporation

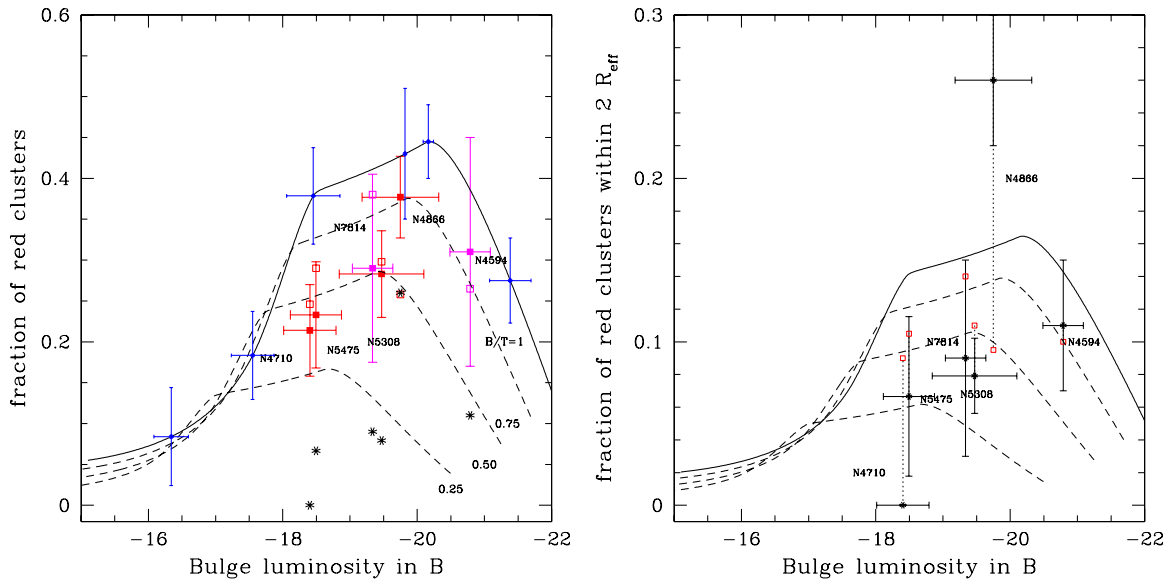


Figure 5. Left: relation between the bulge luminosity in B and the fraction of red GCs. The solid black curve is a fit to the ellipticals (blue circles) from Peng et al. (2008). Black dashed lines represent the expected relation between the bulge luminosity and the fraction of red clusters for $B/T = 0.75, 0.50$, and 0.25 if all the red clusters formed in a manner similar to that in ellipticals. Red and magenta filled squares are the observed values for the target galaxies and comparisons from Goudfrooij et al. (2003) and Spitler et al. (2006), respectively. Open red squares indicate the predicted fraction of red GCs based on their B/T values. Black asterisks show the fraction of red GCs within $2 R_{\text{eff}}$. Right: relation between the bulge luminosity in B and the fraction of red GCs within $2 R_{\text{eff}}$. Black asterisks show the fraction of red GCs within $2 R_{\text{eff}}$ while the red open squares show their predicted fractions based on their B/T values.

rates, are also similar for (bulge) GCs in galaxies with very different bulge luminosities. Over a Hubble time, dynamical friction will destroy GCs within two effective radii of the bulge if they are more massive than $M_{\text{GC}} \gtrsim 3 \times 10^{-6} M_{\text{gal}}$ (where M_{gal} is the total mass of the host galaxy; Gnedin & Ostriker 1997). The largest effect will therefore occur for GCs more massive than $M_{\text{GC}} \gtrsim 1 \times 10^6 M_{\odot}$ in NGC 5475, our lowest luminosity galaxy, with $M_V = -19.72$ ($M_{\text{gal}} \simeq 3 \times 10^{11} M_{\odot}$ assuming $M/L_V = 6.1$ for an Sa galaxy; e.g., Faber & Gallagher 1979). Clusters this massive only represent a fraction $\lesssim 0.09$ of a typical GC mass function. Therefore, we do not expect processes that affect GCs on long timescales to impact the S_N values plotted in Figure 4 at much more than the 10% level, which is smaller than the typical uncertainty in S_N .

Processes that disrupt clusters on shorter ($\tau \lesssim 10^9$ yr) timescales are not as well understood as evaporation and dynamical friction, nor is it known whether the processes which disrupt young clusters in galaxies today are similar to those experienced by GCs during their youth. There is, however, recent evidence which suggests that the early disruption of clusters in nearby galaxies does not vary strongly from galaxy to galaxy (e.g., Fall et al. 2009; Chandar et al. 2010), because it is dominated mainly by processes internal to the clusters themselves. If this was also true for the early evolution of GCs, then disruption processes in general should not have impacted S_N differently from galaxy to galaxy.

The left panel of Figure 5 shows the fraction of red clusters ($f_{\text{red}} = N_{\text{red}}/(N_{\text{red}} + N_{\text{blue}})$) versus bulge luminosity. The solid line shows an empirical relation between f_{red} and bulge luminosity for elliptical galaxies, based on the compilation of Peng et al. (2008), and provides a prediction of f_{red} when bulges form purely via dissipative merging. f_{red} increases with bulge luminosity and then drops off, likely due to the fact that the S_N of blue GCs increases with increasing galaxy luminosity in B (Rhode et al. 2005). Assuming that the number of blue GCs in spirals scales with the total luminosity of the

host galaxy, there should be a factor of $1/(B/T)$ more blue GCs per unit bulge luminosity in spirals relative to ellipticals. Hence, the expected fraction of red GCs in spiral galaxies with different B/T ratios in this dissipative scenario is given by $f_{\text{red,diss}} = N_{\text{red}}/(N_{\text{red}} + N_{\text{blue}} \times 1/(B/T))$. $f_{\text{red,diss}}$ is shown for three different B/T ratios (0.75, 0.50, and 0.25) with dashed lines in Figure 5. Open squares mark values of $f_{\text{red,diss}}$ predicted red GC fractions based on the observed B/T ratios of our sample spirals. The right panel of Figure 5 is a similar plot but for red clusters within $2 R_{\text{eff}}$ of the galaxy bulges, which we derive to be a factor of 0.37 ± 0.10 lower than the total red fraction, using R_{eff} values from Faber et al. (1989) and GC data from Jordán et al. (2009) and Peng et al. (2008).

From Figure 5, we observe the following trends: the fraction of *all* red GCs shows a trend similar to that seen in ellipticals (solid curve). However, comparing the fraction of *all* red GCs to that of *bulge* GCs reveals some intriguing results. Spirals with faint bulges ($M_B > -19.5$ mag) tend to have fractions of red bulge GCs (asterisks in Figure 5) that fall significantly below the values predicted from their B/T ratios (open squares), i.e., below the values expected from purely dissipative processes. However, the fraction of bulge GCs is generally consistent with those expected from merging processes for galaxies with higher-luminosity bulges, NGC 4866 and NGC 4594. NGC 4866 has a relatively large R_{eff} , and the high value observed for the bulge clusters in the right panel of Figure 5 is likely due to the inclusion of some disk clusters.

7. CONCLUSIONS

We have studied four edge-on Sa galaxies and investigated the properties of their GC systems and their relation to their host galaxy bulges. We find that the total number of red clusters as well as the red clusters associated with the bulge in Sa spirals increase with increasing bulge luminosity. However, the bulge S_N of lower-luminosity Sa's are a factor of 2–3 lower than those

of higher-luminosity spirals. We also find that all galaxies in our sample host a blue, presumably old metal-poor GC system with estimated specific frequencies ranging from 0.34 to 0.84, consistent with typical values seen in late-type spirals. We detect a number of red disk clusters in all the sample galaxies. Our results suggest a picture where dissipative processes were more important for building luminous bulges of Sa galaxies, whereas secular evolution may have played a larger role in building lower-luminosity bulges in spirals. More *HST* observations of GC systems in spiral galaxies are needed to verify these results.

We thank the anonymous referee for carefully reading our manuscript and for suggestions which helped to improve this paper. Support for this work was provided by the NASA through *HST* grant GO-10594 from the Space Telescope Science Institute, which is operated by the Association of Universities for Research in Astronomy, Inc., under NASA contract NAS5-26555. T.H.P. acknowledges support in form of the Plaskett Research Fellowship at the Herzberg Institute of Astrophysics of the National Research Council of Canada.

REFERENCES

- Anders, P., & Fritze-v. Alvensleben, U. 2003, *A&A*, 401, 1063
 Ashman, K. M., Bird, C. M., & Zepf, S. E. 1994, *AJ*, 108, 2348
 Bastian, N. 2008, *MNRAS*, 390, 759
 Chandar, R., Whitmore, B. C., & Fall, S. M. 2010, *ApJ*, 713, 1343
 Chandar, R., Whitmore, B. C., & Lee, M. G. 2004, *ApJ*, 611, 220
 Ciotti, L. 1991, *A&A*, 249, 99
 de Vaucouleurs, G. 1953, *MNRAS*, 113, 134
 Dirsch, B., Richtler, T., Geisler, D., Forte, J. C., Bassino, L. P., & Gieren, W. P. 2003, *AJ*, 125, 1908
 Faber, S. M., & Gallagher, J. S., III. 1979, *ARA&A*, 17, 135
 Faber, S. M., Wegner, G., Burstein, D., Davies, R. L., Dressler, A., Lynden-Bell, D., & Terlevich, R. J. 1989, *ApJS*, 71, 173
 Fall, S. M., Chandar, R., & Whitmore, B. C. 2009, *ApJ*, 704, 453
 Fall, S. M., & Zhang, Q. 2001, *ApJ*, 561, 751
 Forbes, D. A., Brodie, J. P., & Larsen, S. S. 2001, *ApJ*, 556, L83
 Gebhardt, K., & Kissler-Patig, M. 1999, *AJ*, 118, 1526
 Georgiev, I. Y., Puzia, T. H., Goudfrooij, P., & Hilker, M. 2010, *MNRAS*, 406, 1967
 Gnedin, O. Y., & Ostriker, J. P. 1997, *ApJ*, 474, 223
 Goudfrooij, P., & de Jong, T. 1995, *A&A*, 298, 784
 Goudfrooij, P., Gilmore, D., Schweizer, F., & Whitmore, B. C. 2004, *ApJ*, 613, L121
 Goudfrooij, P., Mack, J., Kissler-Patig, M., Meylan, G., & Minniti, D. 2001, *MNRAS*, 322, 643
 Goudfrooij, P., Schweizer, F., Gilmore, D., & Whitmore, B. C. 2007, *AJ*, 133, 2737
 Goudfrooij, P., Strader, J., Brennenman, L., Kissler-Patig, M., Minniti, D., & Huizinga, J. E. 2003, *MNRAS*, 343, 665
 Harris, W. E. 1996, *AJ*, 112, 1487
 Harris, W. E., & van den Bergh, S. 1981, *AJ*, 86, 1627
 Jordán, A., et al. 2005, *ApJ*, 634, 1002
 Jordán, A., et al. 2009, *ApJS*, 180, 54
 Kormendy, J., & Kennicutt, R. C., Jr. 2004, *ARA&A*, 42, 603
 Kundu, A., & Whitmore, B. C. 1998, *AJ*, 116, 2841
 Kundu, A., & Whitmore, B. C. 2001, *AJ*, 121, 1251
 Larsen, S. S., Brodie, J. P., Huchra, J. P., Forbes, D. A., & Grillmair, C. J. 2001, *AJ*, 121, 2974
 Maybhate, A., Goudfrooij, P., Schweizer, F., Puzia, T., & Carter, D. 2007, *AJ*, 134, 1729
 Maybhate, A., Goudfrooij, P., Schweizer, F., Puzia, T., & Carter, D. 2009, *AJ*, 137, 383
 McLachlan, G. J., & Basford, K. E. 1988, *Statistics: Textbooks and Monographs* (New York: Dekker)
 McLaughlin, D. E., & Fall, S. M. 2008, *ApJ*, 679, 1272
 Miller, B. W., Whitmore, B. C., Schweizer, F., & Fall, S. M. 1997, *AJ*, 114, 2381
 Peng, E., et al. 2006, *ApJ*, 639, 95
 Peng, E., et al. 2008, *ApJ*, 681, 197
 Pfenniger, D. 1999, *Ap&SS*, 269, 149
 Pfenniger, D., & Norman, C. A. 1990, *ApJ*, 363, 191
 Prieto, J. L., & Gnedin, O. Y. 2008, *ApJ*, 689, 919
 Puzia, T. H., et al. 2004, *A&A*, 415, 123
 Rhode, K. L., & Zepf, S. E. 2004, *AJ*, 127, 302
 Rhode, K. L., Zepf, S. E., Kundu, A., & Larner, A. N. 2007, *AJ*, 134, 1403
 Rhode, K. L., Zepf, S. E., & Santos, M. R. 2005, *ApJ*, 630, L21
 Schweizer, F., Miller, B. W., Whitmore, B. C., & Fall, S. M. 1996, *AJ*, 112, 1839
 Sérsic, J. L. 1963, *BAAA*, 6, 41
 Sheth, K., Vogel, S. N., Regan, M. W., Thornley, M. D., & Teuben, P. J. 2005, *ApJ*, 632, 217
 Spitler, L. R., Larsen, S. S., Strader, J., Brodie, J. P., Forbes, D. A., & Beasley, M. A. 2006, *AJ*, 132, 1593
 Vesperini, E. 2001, *MNRAS*, 322, 247
 Whitmore, B. C., & Schweizer, F. 1995, *AJ*, 109, 960